A GENERALISED RANDOM ENCOUNTER MODEL FOR ESTIMATING ANIMAL DENSITY WITH REMOTE SENSOR DATA

Running title: A generalised random encounter model for animals.

Word count:

Authors:

Tim C.D. Lucas[1,2,3], Elizabeth A. Moorcroft[1,4,5], Robin Freeman[5], Marcus J. Rowcliffe[5], Kate E. Jones[2,5]

Addresses:

1 CoMPLEX, University College London, Physics Building, Gower Street, London, WC1E 6BT, UK

2 Centre for Biodiversity and Environment Research, Department of Genetics, Evolution and Environment, University College London, Gower Street, London, WC1E 6BT, UK

3 Department of Statistical Science, University College London, Gower Street, London, WC1E 6BT, UK

4 Department of Computer Science, University College London, Gower Street, London, WC1E 6BT, UK

5 Institute of Zoology, Zoological Society of London, Regents Park, London, NW1 4RY, UK

Corresponding authors:

Kate E. Jones,
Centre for Biodiversity and Environment Research,
Department of Genetics, Evolution and Environment,
University College London,
Gower Street,
London,
WC1E 6BT,
UK

kate.e.jones@ucl.ac.uk

Marcus J. Rowcliffe,
Institute of Zoology,
Zoological Society of London,
Regents Park,
London,
NW1 4RY,
UK
marcus.rowcliffe@ioz.ac.uk

1. Abstract

1: Wildlife monitoring technology has advanced rapidly and the use of remote sensors such as camera traps, and acoustic detectors is becoming common in both the terrestrial and marine environments. Current capture-recapture or distance methods to estimate abundance or density require individual recognition of animals or knowing the distance of the animal from the sensor, which is often difficult. A method without these requirements, the random encounter model (REM), has been successfully applied to estimate animal densities from count data generated from camera traps. However, count data from acoustic detectors do not fit the assumptions of the REM due to the directionality of animal signals.

2: We developed a generalised REM (gREM), to estimate absolute animal density from count data from both camera traps and acoustic detectors. We derived the gREM for different combinations of sensor detection widths and animal signal widths (a measure of directionality). We tested the accuracy and precision of this model using simulations of different combinations of sensor detection widths and animal signal widths, number of captures, and models of animal movement.

3: We find that the gREM produces accurate estimates of absolute animal density for all combinations of sensor detection widths and animal signal widths. However, larger sensor detection and animal signal widths were found to be more precise. While the model is accurate for all capture efforts tested, the precision of the estimate increases with the number of captures. We found no effect of different animal movement models tested on the accuracy and precision of the gREM.

4: We conclude that the gREM provides an effective method to estimate absolute animal densities from remote sensor count data over a range of sensor and animal signal widths. The gREM is applicable for use for count data obtained in both marine and terrestrial environments, visually or acoustically (e.g., big cats, sharks, birds, bats and cetaceans). As sensors such as camera traps and acoustic detectors become more ubiquitous, the gREM will be increasingly useful for monitoring animal populations across broad spatial, temporal and taxonomic scales.

1.1. **Keywords.** Acoustic detection, Camera traps, Marine, Population monitoring, Simulations, Terrestrial

2. Introduction

Animal population density is one of the fundamental measures needed in ecology and conservation. The density of a population has important implications for a range of issues such as sensitivity to stochastic fluctuations (Richter-Dyn & Goel, 1972; Wright & Hubbell, 1983) and risk of extinction (Purvis *et al.*, 2000). Monitoring animal population changes in response to anthropogenic pressure is becoming increasingly important as humans modify habitats and change climates as never before (Everatt *et al.*, 2014). Sensor technology, such as camera traps (Rowcliffe & Carbone, 2008; Karanth, 1995) and acoustic detectors (O'Farrell & Gannon, 1999; Clark, 1995; Acevedo & Villanueva-Rivera, 2006) are becoming increasingly used to monitor changes in animal populations (Rowcliffe & Carbone, 2008; Kessel *et al.*, 2014), as they are efficient, relativity cheap and non-invasive (Cutler & Swann, 1999), allowing for surveys over large areas and long periods. However, the problem of converting sampled count data to estimates of density remains as efforts must be made to account for detectability of the animals (Anderson, 2001).

Methods do already exist for estimating animal density if the distance between the animal and the sensor can be estimated (e.g., capture-mark recapture methods (Karanth, 1995) and distance sampling (Harris *et al.*, 2013)). However, these methods often require additional information that may not be available. For example, capture-mark-recapture methods (Karanth, 1995; Trolle & Kéry, 2003; Soisalo & Cavalcanti, 2006; Trolle *et al.*, 2007) require recognition of individuals; distance methods require a distance estimation of how far away individuals are from the sensor barlow2005estimates, marques2011estimating. The development of the random encounter model (REM) (a modification of a gas model) enabled animal densities to be estimated from unmarked individuals of a known speed, and sensor detection parameters (Rowcliffe *et al.*, 2008). The REM method has been successfully applied to estimate animal densities from camera trap surveys (Manzo *et al.*, 2012; Zero *et al.*, 2013). However, extending the REM method to other types of sensors (for example acoustic detectors) is more problematic, because the original derivation assumes a relatively narrow sensor width (up to $\pi/2$ radians) and that the animal is equally detectable irrespective of its heading (ref).

Whilst these restrictions are not problematic for most camera trap makes (e.g. Reconyx, Cuddeback), the REM could not be used to estimate densities from camera traps with a wider sensor width (e.g. canopy monitoring with fish eye lens (Brusa & Bunker, 2014)). Additionally, the REM method would not be useful in estimating densities from acoustic survey data as the acoustic detector angles are often wider than $\pi/2$ radians. Acoustic detectors are designed for a range of diverse tasks and environments (Kessel *et al.*, 2014), which will naturally lead to a wide range of sensor detection widths and detection distances. In addition to this, calls emitted by many animals are directional (breaking the assumption of the REM method).

There has been a sharp rise in interest around passive acoustic detectors in recent years, with a 10 fold increase in publications in the decade between 2000 and 2010 (Kessel *et al.*, 2014). Acoustic monitoring is being developed to study many aspects of ecology, including the interactions of animals and their environments (Blumstein *et al.*, 2011; Rogers *et al.*, 2013), the presence and relative abundances of species (Marcoux *et al.*, 2011), and biodiversity of an area (Depraetere *et al.*, 2012).

Acoustic data suffers from many of the problems associated with data from camera trap surveys in that individuals are often unmarked so capture-make-recapture methods cannot be used to estimate densities. In some cases the distance between the animal and the sensor is known, for example when an array of sensors and the position of the animal is estimated by triangulation (Lewis *et al.*, 2007). In these situations distance-sampling methods can be applied, a method typically used for marine mammals (Rogers *et al.*, 2013). However, in many cases distance estimation is not possible, for example when single sensors are deployed, a situation typical in the majority of terrestrial acoustic surveys (Elphick, 2008; Buckland *et al.*, 2008). In these cases, only relative measures of local abundance can be calculated, and not absolute densities. This means that comparison of populations between species and sites is problematic without assuming equal detectability (Schmidt, 2003). Equality detectability is unlikely because of differences in environmental conditions, sensor type, habitats, species biology.

In this study we create a generalised REM (gREM), as an extension to the camera trap model of (Rowcliffe *et al.*, 2008), to estimate absolute density from count data from acoustic detectors, or camera traps, where the sensor width can vary from 0 to 2π radians, and the signal given off from the animal can be directional. We assessed the accuracy and precision of the gREM within a simulated environment, by varying the sensor detection widths, animal signal widths, number of captures and models of animal movement. We use the simulation results to recommend best survey practice for estimating animal densities from remote sensors.

3. Methods

3.1. **Analytical Model.**

The REM presented by (Rowcliffe *et al.*, 2008) adapts the gas model to model count data from camera trap surveys. The REM is derived assuming a stationary sensor with a detection width θ less than $\pi/2$ radians and detection distance r (Appendix S1 for a list of symbols), giving a circular sector within which animals can be captured (the detection zone)(Figure 1). However, in order to apply this approach more generally, and in particular to acoustic detectors, we need both to relax the constraint on sensor detection width, and allow for animals with directional signals. We therefore model the animal as having an associated signal width α (Figure 1). Consequently, we derive the gREM for any detection width, θ, between 0 and 2π and any signal width, α, between 0 and 2π. We start deriving the gREM with the simplest situation, the gas model where $\theta = 2\pi$ and $\alpha = 2\pi$.

3.1.1. *Gas Model.*

Following Yapp (1956), we derive the gas model where sensors can capture animals in any direction and animals give out signals in all directions ($\theta = 2\pi$ and $\alpha = 2\pi$). We assume that animals are in a homogeneous environment, and move in straight lines of random direction with velocity v. We allow that our stationary sensor can capture animals at a detection distance r and that if an animal moves within this detection zone they are captured with a probability of one, while animals outside the zone are never captured.

For derivation purposes, we consider relative velocity from the reference frame of the animals. Conceptually, this requires us to imagine that all animals are stationary and randomly distributed in space, while the sensor moves with velocity

v. If we calculate the area covered by the sensor during the survey period we can estimate the number of animals it should capture. As a circle moving across a plane, the area covered by the sensor per unit time is $2rv$. The number of expected captures, z, for a survey period of t, with an animal density of D is $z = 2rvtD$. To estimate the density, we rearrange to get $D = z/2rvt$.

3.1.2. *gREM derivations for different detection and signal widths.* Different combinations of θ and α would be expected to occur (e.g., sensors have different detection widths and animals have different signal widths). For different combinations θ and α, the area covered per unit time is no longer given by $2rv$. Instead of the size of the sensor detection zone having a diameter of $2r$, the size changes with the approach angle between the sensor and the animal. For any given signal width and detector width and depending on the angle that the animal approaches the sensor, the width of the area within which an animal can be detected is called the profile, p. The size of the profile (averaged across all approach angles) is defined as the average profile $\bar{p}$. However, different combinations of θ and α need different equations to calcuate $\bar{p}$.

We have identified the parameter space for the combinations of θ and α for which the derivation of the equations are the same (defined as sub-models in the gREM) (Figure 2). For example, the gas model becomes the simplest gREM sub-model (upper right in (Figure 2) and the REM from (Rowcliffe *et al.*, 2008) is another gREM sub-model where $\theta < \pi/2$ and $\alpha = 2\pi$. We derive one gREM sub-model SE2 as an example below (where $4\pi - 2\alpha < \theta < 2\pi,\ 0 < \alpha < \pi$) (see Appendix S2 for other gREM sub-models).

3.1.3. *Example derivation of SE2.* In order to calculate the size of the average profile, we have to integrate over the focal angle, x_1 (Figure 3a). This is the angle taken from the centre line of the sensor. Other focal angles are possible (x_2, x_3, x_4) and are used in other gREM sub-models (see Appendix S2). As the size of the profile depends on the approach angle, we present the derivation across all approach angles. When the sensor is directly approaching the animal $x_1 = \pi/2$.

Starting from $x_1 = \pi/2$ the size of profile is $2r \sin \alpha/2$ (Figure 3b). At this point, the size of α limits the size of the profile. This remains the case until the animal reaches the right hand side of the sensor where $x_1 = \theta/2 + \pi/2$ - $\alpha/2$ (Figure 3c). When the sensor is approached from this angle the size of the profile is $r\sin(\alpha/2) + r\cos(x_1 - \theta/2)$ and the size of $\theta/$ limits the size of the profile. Finally, at $x_1 = 5\pi/2 - \theta/2 - \alpha/2$ an animal can again be detected from the right side of the detector; the approach angle is far enough round to see past the 'blind spot' of the sensor. In this region, until $x_1 = 3\pi/2$, the width of the profile is again $2r\sin\alpha/2$ (Figure 3d).

We have therefore characterised the profile width for π radians of rotation (from directly towards the sensor to directly behind the sensor). To find the average profile width for all angles of approach, we integrate these functions over their appropriate intervals of x_1 and divide by π to give:

$$\begin{aligned}\bar{p} &= \frac{1}{\pi}\left(\int_{\frac{\pi}{2}}^{\frac{\pi}{2}+\frac{\theta}{2}-\frac{\alpha}{2}} 2r\sin\frac{\alpha}{2}\,\mathrm{d}x_1 + \int_{\frac{\pi}{2}+\frac{\theta}{2}-\frac{\alpha}{2}}^{\frac{5\pi}{2}-\frac{\theta}{2}-\frac{\alpha}{2}} r\sin\frac{\alpha}{2} + r\cos\left(x_1 - \frac{\theta}{2}\right)\mathrm{d}x_1 + \int_{\frac{5\pi}{2}-\frac{\theta}{2}-\frac{\alpha}{2}}^{\frac{3\pi}{2}} 2r\sin\frac{\alpha}{2}\,\mathrm{d}x_1\right)\\ &= \frac{r}{\pi}\left(\theta\sin\frac{\alpha}{2} - \cos\frac{\alpha}{2} + \cos\left(\frac{\alpha}{2}+\theta\right)\right) \qquad \text{eqn 1}\end{aligned}$$

Here the three integrals correspond to Figures 3b, 3c and 3d respectively. Then, as with the gas model, this term is used to calculate density

$$D = z/vt\bar{p} \qquad \text{eqn 2}$$

We can also see what causes this model to be discontinuously different to SE3. Examine the profile at $x_1 = \theta/2 + \pi/2$ (the profile is perpendicular to the edge of the blind spot.) We see that there is potentially a case where the left side of the profile is $r\sin\alpha/2$ while the right side is zero. This profile does not exist if we return to the full $2r\sin\alpha/2$ profile before $x_1 = \theta/2 + \pi/2$. Therefore we solve $5\pi/2 - \theta/2 - \alpha/2 < \theta/2 + \pi/2$. We find that this new profile only exists if $\alpha < 4\pi - 2\theta$. This inequality defines the line separating models SE2 and its neighbouring model, SE3.

While specification of the models had to be done by hand, the calculation of the solutions was done using SymPy (SymPy Development Team, 2014) in Python. The models were checked for errors with a number of tests. The models were checked against each other by checking that models which are adjacent in parameter space are equal at the boundary between them (e.g., eqn 1 is equal to 2r as in the gas model when $\alpha = \pi$ and $\theta = 2\pi$). Models that border $\alpha = 0$ should have $p = 0$ when $\alpha = 0$ and this was checked for (e.g., eqn 1 is 0 when $\alpha = 0$ and $\theta = 2\pi$). We checked that all solutions are between 0 and $2r$ and that each integral, divided by the range of angles that it is integrated over is between 0 and $2r$. These tests are included in Appendix S3), and all derivations in full are included in Appendix S2 with computer algebra scripts in Appendix S3, and the R (R Development Core Team, 2010) script for the gREM in Appendix S4.

3.2. **Simulation Model.** In order to validate the gREM we developed a spatially explicit simulation of animal movement. By simulating animal movement with various movement patterns within a continuous space containing sensors we calculated how many animal contacts the sensors would have detected.

Each simulation consisted of a 7.5 km by 7.5 km square (with periodic boundaries) and was populated with a density of 70 animals km^{-2} to match an expected maximum density of mammals in the wild (Damuth, 1981), creating a total of 3937 animals per simulation which were placed randomly at the start of the simulation. Animal movement was simulated with a simple movement model, characterised by a random movement distance for each discrete time step, at the end of each step the animal could change direction with a uniform distribution up to a maximum specified angle. The simulation lasted for N steps of duration T during which the animals moved with an average speed, v. The distance travelled in each time step, d, was sampled from a Normal distribution with mean distance, $\mu_d = vT$, and standard deviation $\sigma_d = vT/10$. An average speed, $v = 40\,\text{km days}^{-1}$, was chosen as this represents the largest day range of terrestrial animals (Carbone *et al.*, 2005), and represents the upper limit of realistic speeds. To reduce computation effort, a single set of 100 simulations was run for a long duration which could be subsampled.

Animals were counted as they moved in and out of the detection zone of stationary detectors in the simulation. Multiple detectors were set up in each simulation with varying detection angles with the results recorded separately. The details of each individual capture event, including the angle between the animals heading and the sensor, were saved from this information the number of capture events can be calculated for a given call angle. The total number of these detections were summed for each set of parameters in the simulation, the gREM was then applied in order to estimate the density in the simulation. The difference between the true input density and density estimated by the gREM were used to evaluate the bias in the analytical models. If the gREM is correct the mean difference between the two values were expected to converge to zero as sample size increases. For each of the 100 simulations we calculate the error (the difference between the known and estimated density) and so we got a distribution of errors which was approximately normal. We constructed boxplots of the estimates error to graphically test for significant differences between the true and estimated densities.

All the derived models were tested to demonstrate the accuracy and precision of the gREM while the assumptions of the analytical models were met. We selected four example models (models NW1, SW1, NE1, and SE3, as in Figure 2) for demonstrating the accuracy and precision of the gREM with low captures rates, and the accuracy and precision when movement patterns brake the assumptions of the gREM. We specifically looked at a non-continuous movement, and a range of correlated random walks, both of which would be seen in real field conditions. The four models were chosen as they represent one model from each quadrant of Figure 4. The accuracy and precision of all the derived models in the gREM follow the same pattern as the four that have been shown in the main text.

4. Results

4.1. **Analytical model.** Model results have been derived for each zone with all models except the gas model and REM being newly derived here. However, many models, although derived separately, have the same expression for p. Figure 4 shows the expression for p in each case. The general equation for density, using the correct expression for p is then substituted into eqn 2.

Although more thorough checks are performed in Appendix S3, it can be seen that all adjacent expressions in Figure 4 are equal when expressions for the boundaries between them are substituted in.

4.2. **Simulation model.** For each model we compared the estimated densities to the true densities in a simulation. None of the models showed any evidence of any significant differences between the estimated and true density values (Figure 5). The precision of the models do vary however. The standard deviation of the error is strongly related to the call and sensor width (Figure 6), such that larger widths have greater precision. However, even the models with small call and sensor angles have a relativity high level of precision.

The precision of the model is dependent on the number of captures during the survey. In Figure 8 we can see that the model precision gets greater as the number of captures increase. As the number of captures reaches about 100 then the coefficient of variation falls below 10% which could be considered negligible.

4.2.1. *Use of the gREM when animal movement is not consistent with model assumptions.* Simulating start-stop instead of continuous movement had no effect the accuracy, or the precision, of the estimates (Figure 10) as long as the true overall speed of the animal is known. Relaxing straight line movement to allow random or correlated random walks did not effect the accuracy of the method (Figure 12). We allowed animals to change direction up to a maximum value at the end of each step, picked from a uniform distribution where the maximum angle ranged from 0 to π, which corresponds to straight line movement and random walk respectively. There is no significant difference in the variance for the change, this could be because of the between the step length of the animal movement, 15 minutes, means that immediate double counting of the same animal is unlikely. In the case where large directional changes are likely to occur within short periods of time leading to double counting of the same animal within a short period of time may need to be adjusted because of this.

5. Discussion

We have developed the gREM such that it can be used to estimate density from acoustic and optical sensors. This has entailed a generalisation of the gas model and the model in (Rowcliffe *et al.*, 2008) to be applicable to any combination of sensor width and call directionality. We have used simulations to show, as a proof of principle, that these models are accurate and precise.

The gREM is therefore available for the estimation of density of a number of taxa of importance to conservation, zoonotic diseases and ecosystem services. The models provided are suitable for certain groups for which there are currently no, or few, effective methods for density estimation. Any species that would be consistently recorded at least once when within range of a detector would be a suitable subject for the gREM, such as bats (Kunz *et al.*, 2009), songbirds (Buckland & Handel, 2006), Cetaceans (Marques *et al.*, 2009) or forest primates (Hassel-Finnegan *et al.*, 2008). Within increasing technological capabilities, this list of species is likely to increase dramatically.

Importantly the methods are noninvasive and do not require human marking or naturally identifying marks (as required for mark-recapture models). This makes them suitable for large, continuous monitoring projects with limited human resources. It also makes them suitable for species that are under pressure, species that cannot naturally be individually recognised or species that are difficult or dangerous to catch.

From our simulations we believe that this method has the potential produce accurate and precise estimates for many different species, using either camera or acoustic detectors. When choosing detectors a researcher should pick the detector with the largest radius and detection angle possible, but whilst a small capture area may reduce precision there is only a limited impact on the overall precision of the model (Figure 6). A range of factors will affect the overall precision of the model, like size of detection zone, speed of animal, density of animals and length of survey which are reflected in the number of captures. Increasing the number of captures leads to more precise estimates, for species which more slower, or have occur at lower densities, then the detection zone and length of survey need to be increased to compensate so that at least 100 captures are collected (Figure 8).

Within the simulation we have assumed an equal density across the entire world, however in a field environment the situation would be much more complex, with additional variation coming from local changes in density between camera sites. We also assume perfect knowledge of the average speed of an animal and size of the detection zone, and instant triggering of the camera. All of which may lead to possible bias or decreased precision.

Although we have used simulations to validate these models, much more robust testing is needed. Although difficult, proper field test validation would be required before the models could be fully trusted. Note, however, that the REM (Rowcliffe *et al.*, 2008) has been field tested. Both Rowcliffe *et al.* (2008) and Zero *et al.* (2013) both found that the REM were effective manner of estimating animal densities (Rowcliffe *et al.*, 2008; Zero *et al.*, 2013). There was some discrepancies between the REM and the census methodologies found by Rovero and Marshall which may have been down to lack of knowledge of wild animal speed, and an underestimate in census results (Rovero & Marshall, 2009). In some taxa gold standard methods of estimating animal density exist, such as capture mark recapture. Where these gold standard exist, and have been proved to work, a simultaneous gREM study could be completed to test the accuracy under field conditions. An easier way to continue to evaluate the models is to run more extensive simulations which break the assumptions of the analytical models. The main element that cannot be analytically treated is the complex movement of real animals. Therefore testing these methods against true animal traces, or more complex movement models would be useful.

There are a number of positive extensions to the gREM which could be developed in the future. The original gas model was formulated for the case where both subjects, either animal and detector, or animal and animal, are moving (Hutchinson & Waser, 2007). Indeed any of the models with animals that are equally detectable in all directions ($\alpha = 2\pi$) can be trivially expanded for moving by substituting the sum of the average animal velocity and the sensor velocity for v as used here. However, when the animal has a directional call, the extension becomes much less simple. The approach would be to calculate again the mean profile width. However, for each angle of approach, one would have to average the profile width for an animal facing in any direction (i.e. not necessarily moving towards the sensor) weighted by the relative velocity of that direction. There are a number of situations where a moving detector and animal could occur and as such may be advantage to have a method of estimating densities from the data collected, e.g. an acoustic detector based off a boat when studying Cetacea or sea birds (Yack *et al.*, 2013).

Another interesting, and so far unstudied problem, is edge effects caused by trigger delays (the delay between sensing an animal and attempting to record the encounter) and time expansion acoustic detectors which repeatedly turn on an off during sampling. Both of these have potential biases as animals can move through the detection zone without being detected. The models herein are formulated assuming constant surveillance and so the error quickly becomes negligible. For example, if it takes longer for the recording device to be switched on than the length of some animal calls there could be a systematic underestimation of density.

6. Acknowledgments

References

Acevedo, M.A. & Villanueva-Rivera, L.J. (2006) Using automated digital recording systems as effective tools for the monitoring of birds and amphibians. *Wildlife Society Bulletin*, **34**, 211–214.

Anderson, D.R. (2001) The need to get the basics right in wildlife field studies. *Wildlife Society Bulletin*, pp. 1294–1297.

Blumstein, D.T., Mennill, D.J., Clemins, P., Girod, L., Yao, K., Patricelli, G., Deppe, J.L., Krakauer, A.H., Clark, C., Cortopassi, K.A. *et al.* (2011) Acoustic monitoring in terrestrial environments using microphone arrays: applications, technological considerations and prospectus. *Journal of Applied Ecology*, **48**, 758–767.

Brusa, A. & Bunker, D.E. (2014) Increasing the precision of canopy closure estimates from hemispherical photography: Blue channel analysis and under-exposure. *Agricultural and Forest Meteorology*, **195**, 102–107.

Buckland, S.T. & Handel, C. (2006) Point-transect surveys for songbirds: robust methodologies. *The Auk*, **123**, 345–357.

Buckland, S.T., Marsden, S.J. & Green, R.E. (2008) Estimating bird abundance: making methods work. *Bird Conservation International*, **18**, S91–S108.

Carbone, C., Cowlishaw, G., Isaac, N.J. & Rowcliffe, J.M. (2005) How far do animals go? Determinants of day range in mammals. *The American Naturalist*, **165**, 290–297.

Clark, C.W. (1995) Application of US Navy underwater hydrophone arrays for scientific research on whales. *Reports of the International Whaling Commission*, **45**, 210–212.

Cutler, T.L. & Swann, D.E. (1999) Using remote photography in wildlife ecology: a review. *Wildlife Society Bulletin*, pp. 571–581.

Damuth, J. (1981) Population density and body size in mammals. *Nature*, **290**, 699–700.

Depraetere, M., Pavoine, S., Jiguet, F., Gasc, A., Duvail, S. & Sueur, J. (2012) Monitoring animal diversity using acoustic indices: implementation in a temperate woodland. *Ecological Indicators*, **13**, 46–54.

Elphick, C.S. (2008) How you count counts: the importance of methods research in applied ecology. *Journal of Applied Ecology*, **45**, 1313–1320.

Everatt, K.T., Andresen, L. & Somers, M.J. (2014) Trophic scaling and occupancy analysis reveals a lion population limited by top-down anthropogenic pressure in the limpopo national park, mozambique. *PloS one*, **9**, e99389.

Harris, D., Matias, L., Thomas, L., Harwood, J. & Geissler, W.H. (2013) Applying distance sampling to fin whale calls recorded by single seismic instruments in the northeast atlantic. *The Journal of the Acoustical Society of America*, **134**, 3522–3535.

Hassel-Finnegan, H.M., Borries, C., Larney, E., Umponjan, M. & Koenig, A. (2008) How reliable are density estimates for diurnal primates? *International Journal of Primatology*, **29**, 1175–1187.

Hutchinson, J.M.C. & Waser, P.M. (2007) Use, misuse and extensions of "ideal gas" models of animal encounter. *Biological Reviews of the Cambridge Philosophical Society*, **82**, 335–359.

Karanth, K. (1995) Estimating tiger (*Panthera tigris*) populations from camera-trap data using capture–recapture models. *Biological Conservation*, **71**, 333–338.

Kessel, S., Cooke, S., Heupel, M., Hussey, N., Simpfendorfer, C., Vagle, S. & Fisk, A. (2014) A review of detection range testing in aquatic passive acoustic telemetry studies. *Reviews in Fish Biology and Fisheries*, **24**, 199–218.

Kunz, T.H., Betke, M., Hristov, N.I. & Vonhof, M. (2009) Methods for assessing colony size, population size, and relative abundance of bats. *Ecological and behavioral methods for the study of bats (TH Kunz and S Parsons, eds) 2nd ed Johns Hopkins University Press, Baltimore, Maryland*, pp. 133–157.

Lewis, T., Gillespie, D., Lacey, C., Matthews, J., Danbolt, M., Leaper, R., McLanaghan, R. & Moscrop, A. (2007) Sperm whale abundance estimates from acoustic surveys of the ionian sea and straits of sicily in 2003. *Journal of the Marine Biological Association of the United Kingdom*, **87**, 353–357.

Manzo, E., Bartolommei, P., Rowcliffe, J.M. & Cozzolino, R. (2012) Estimation of population density of european pine marten in central italy using camera trapping. *Acta Theriologica*, **57**, 165–172.

Marcoux, M., Auger-Méthé, M., Chmelnitsky, E.G., Ferguson, S.H. & Humphries, M.M. (2011) Local passive acoustic monitoring of narwhal presence in the canadian arctic: a pilot project. *Arctic*, pp. 307–316.

Marques, T.A., Thomas, L., Ward, J., DiMarzio, N. & Tyack, P.L. (2009) Estimating cetacean population density using fixed passive acoustic sensors: An example with Blainville's beaked whales. *The Journal of the Acoustical Society of America*, **125**, 1982–1994.

O'Farrell, M.J. & Gannon, W.L. (1999) A comparison of acoustic versus capture techniques for the inventory of bats. *Journal of Mammalogy*, pp. 24–30.

Purvis, A., Gittleman, J.L., Cowlishaw, G. & Mace, G.M. (2000) Predicting extinction risk in declining species. *Proceedings of the Royal Society of London Series B: Biological Sciences*, **267**, 1947–1952.

R Development Core Team (2010) *R: A Language And Environment For Statistical Computing*. R Foundation For Statistical Computing, Vienna, Austria. ISBN 3-900051-07-0.

Richter-Dyn, N. & Goel, N.S. (1972) On the extinction of a colonizing species. *Theoretical Population Biology*, **3**, 406–433.

Rogers, T.L., Ciaglia, M.B., Klinck, H. & Southwell, C. (2013) Density can be misleading for low-density species: benefits of passive acoustic monitoring. *Public Library of Science One*, **8**, e52542.

Rovero, F. & Marshall, A.R. (2009) Camera trapping photographic rate as an index of density in forest ungulates. *Journal of Applied Ecology*, **46**, 1011–1017.

Rowcliffe, J.M. & Carbone, C. (2008) Surveys using camera traps: are we looking to a brighter future? *Animal Conservation*, **11**, 185–186.

Rowcliffe, J., Field, J., Turvey, S. & Carbone, C. (2008) Estimating animal density using camera traps without the need for individual recognition. *Journal of Applied Ecology*, **45**, 1228–1236.

Schmidt, B.R. (2003) Count data, detection probabilities, and the demography, dynamics, distribution, and decline of amphibians. *Comptes Rendus Biologies*, **326**, 119–124.

Soisalo, M.K. & Cavalcanti, S. (2006) Estimating the density of a jaguar population in the Brazilian Pantanal using camera-traps and capture-recapture sampling in combination with GPS radio-telemetry. *Biological Conservation*, **129**, 487–496.

SymPy Development Team (2014) *SymPy: Python library for symbolic mathematics*.

Trolle, M. & Kéry, M. (2003) Estimation of ocelot density in the Pantanal using capture-recapture analysis of camera-trapping data. *Journal of mammalogy*, **84**, 607–614.

Trolle, M., Noss, A.J., Lima, E.D.S. & Dalponte, J.C. (2007) Camera-trap studies of maned wolf density in the Cerrado and the Pantanal of Brazil. *Biodiversity and Conservation*, **16**, 1197–1204.

Wright, S.J. & Hubbell, S.P. (1983) Stochastic extinction and reserve size: a focal species approach. *Oikos*, pp. 466–476.

Yack, T.M., Barlow, J., Calambokidis, J., Southall, B. & Coates, S. (2013) Passive acoustic monitoring using a towed hydrophone array results in identification of a previously unknown beaked whale habitat. *The Journal of the Acoustical Society of America*, **134**, 2589–2595.

Yapp, W. (1956) The theory of line transects. *Bird study*, **3**, 93–104.

Zero, V.H., Sundaresan, S.R., O'Brien, T.G. & Kinnaird, M.F. (2013) Monitoring an endangered savannah ungulate, Grevy's zebra (*Equus grevyi*): choosing a method for estimating population densities. *Oryx*, **47**, 410–419.

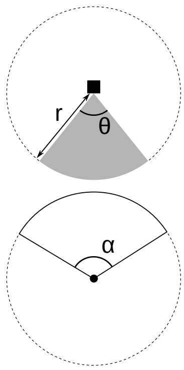

FIGURE 1. Representation of sensor detection width and animal signal width. The filled square and circle represent a sensor and an animal, respectively; θ, sensor detection width (radians); r, sensor detection distance; dark grey shaded area, sensor detection zone; α, animal signal width (radians). Dashed lines around the filled square and circle represents the maximum extent of θ and α, respectively.

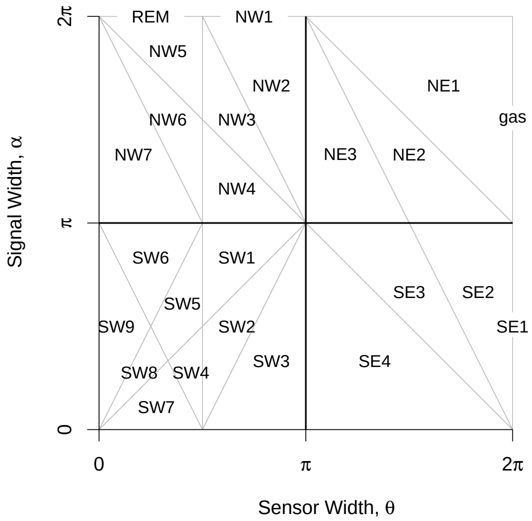

FIGURE 2. The locations of gREM submodels in parameter space. Each polygon shows the parameter space (combination of sensor detection width and animal signal width) for which a given gREM submodel is needed. The submodels are named after the compass point of the quadrant they are in.

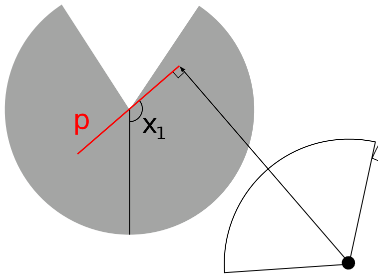

(A) Location of x_1

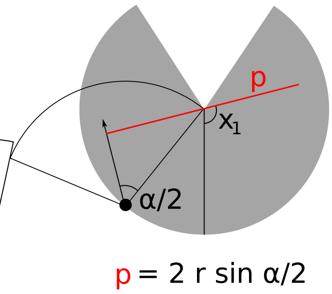

(B) First integral

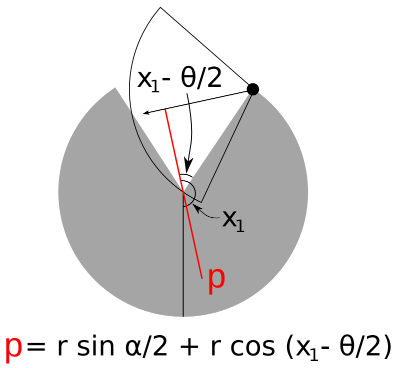

(C) Second Integral

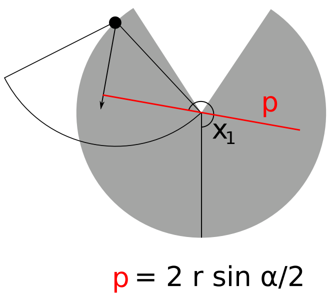

(D) Third Integral

FIGURE 3. Representation of size of the detection zone presented to the animal by the sensor for a focal angle of x_1 for (a) directly approaching blah, (b) blah, and (c) blah. The filled square and circle represent a sensor and an animal, respectively; dark grey shaded area, sensor detection zone; red line, size of the detection zone presented to the animal; x_1, focal angle; and the dashed arrow represents the movement of the sensor.

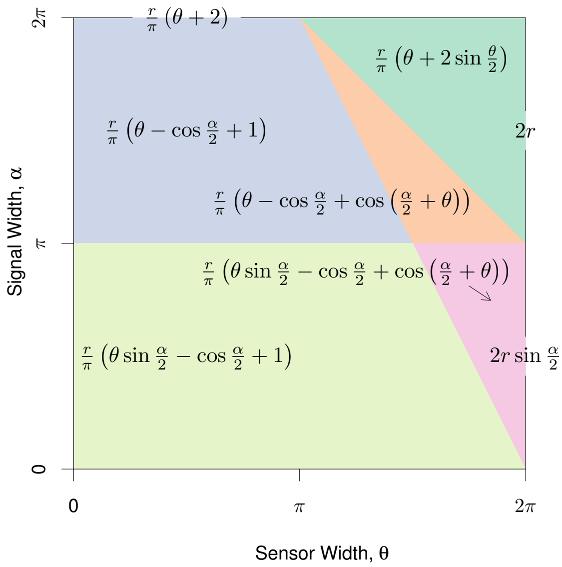

FIGURE 4. Equations for the profile wide, p, given sensor and call widths. Each colour block represents one equation, despite independent derivation within each block, many models result in the same expression. These are collected together and presented as one block of colour.

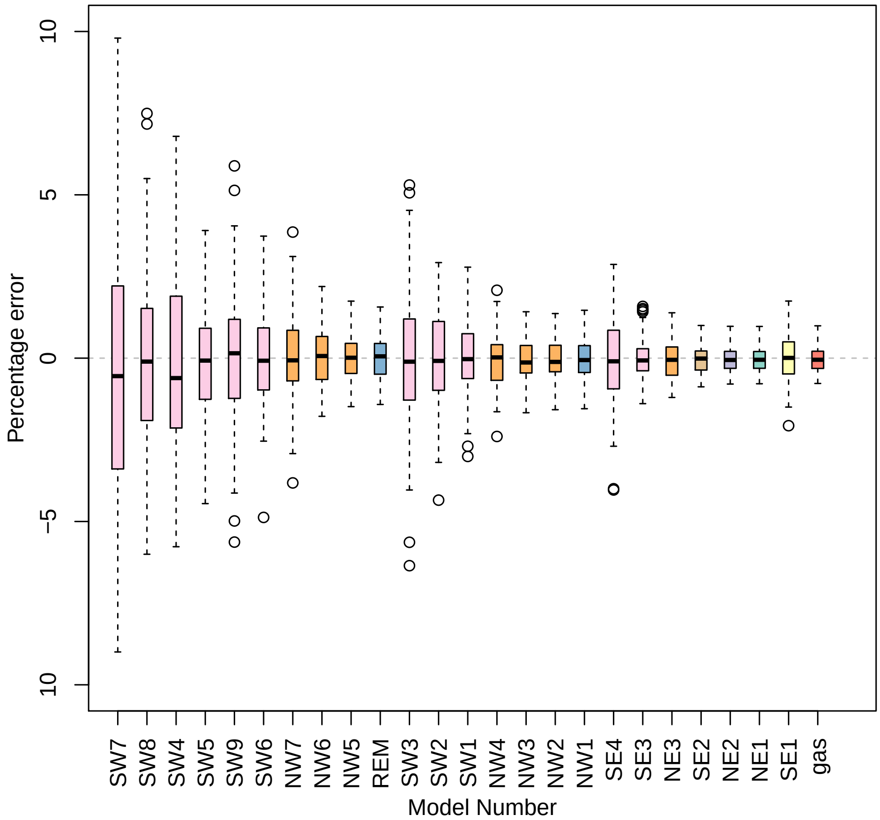

FIGURE 5. Distribution of the bias for each of the derived models. Percentage error of analytical model calculated from the simulation when settings are: r = 100 m; T = 150 days; v = 40 km days^{-1}; D = 70 animals km^{-2}; and with detection angles varying between models. The numbers referred to here can be found in Figure 1 Appendix S2, and the colour of each box plot match the functional form of the equation as seen in Figure 4.

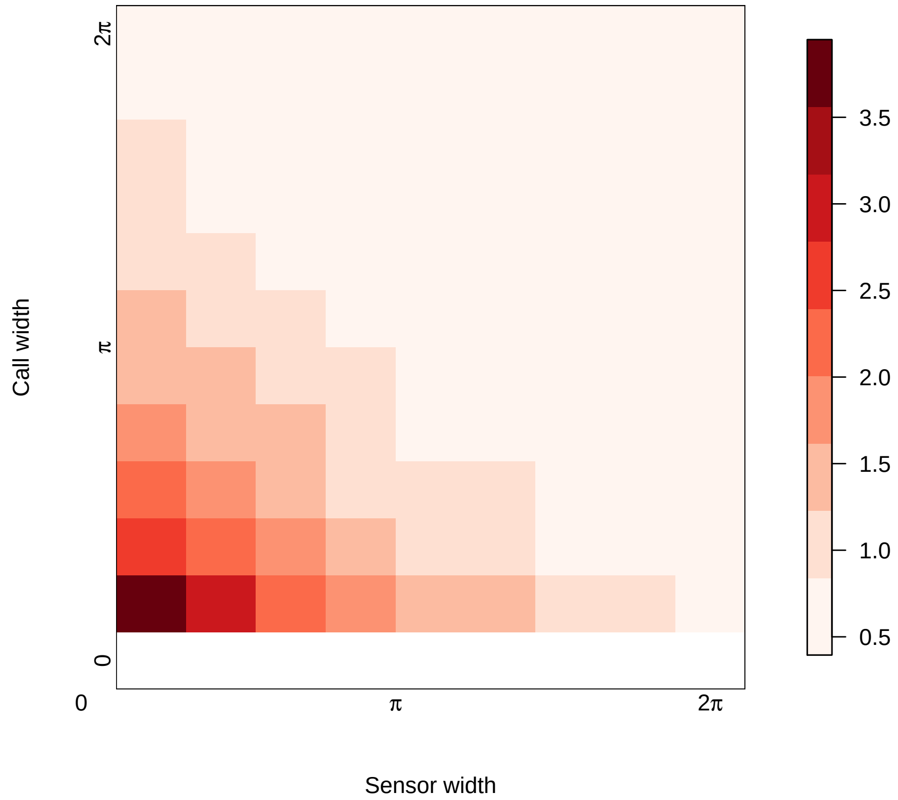

FIGURE 6. Angle of detector

FIGURE 7. The precision of the gREM given a range of detection and call angles. The standard deviation of the percentage error for sensor, and call angles between 0 and 2π where: $r = 100\,\mathrm{m}$; $T = 150\,\mathrm{days}$; $v = 40\,\mathrm{km\,days}^{-1}$; $D = 70\,\mathrm{animals\,km}^{-2}$; and with detection angles varying between models. Where red indicates a high standard deviation and blue represents a low standard deviation.

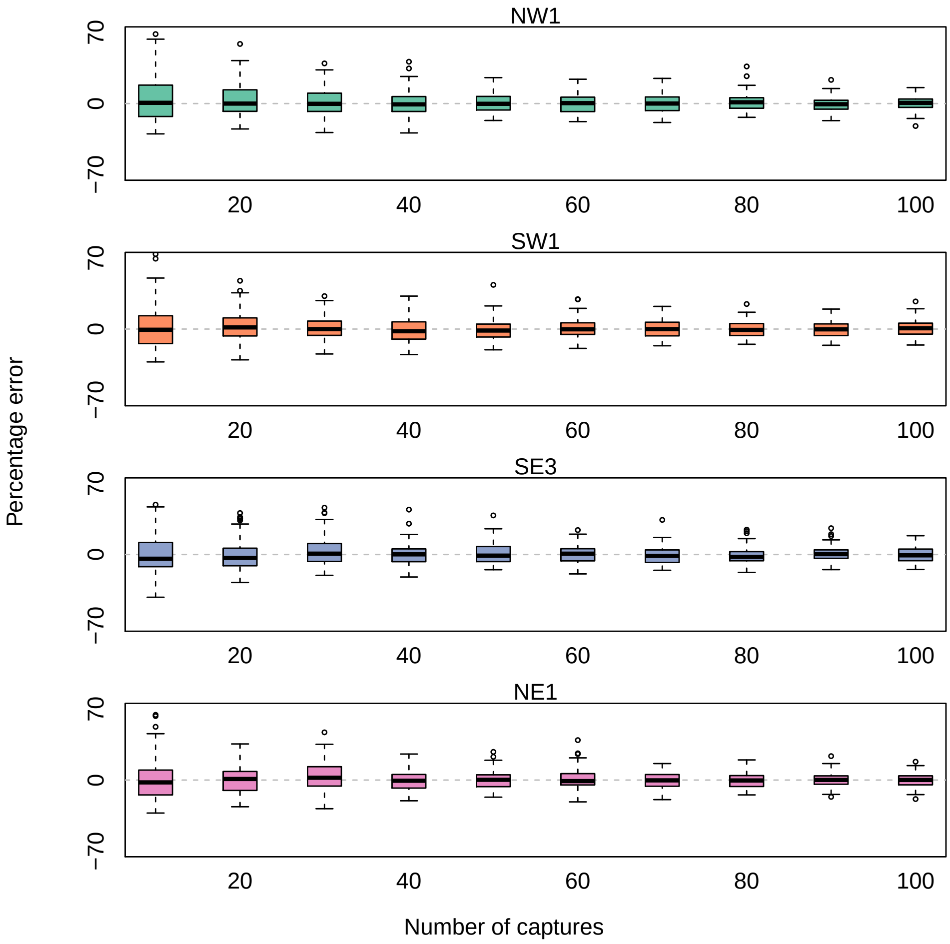

FIGURE 8. Number of captures

FIGURE 9. Accuracy of the gREM reminds unchanged, whilst precision increases, with captures. Boxplots of four test models when given different numbers of captures where: $r = 100\,\mathrm{m}$; $T = 150$ days; $v = 40\,\mathrm{km\,days}^{-1}$; $D = 70$ animals km^{-2}; and with angles varying between models. Where the model names refer to Figure 1 in Appendix S2.

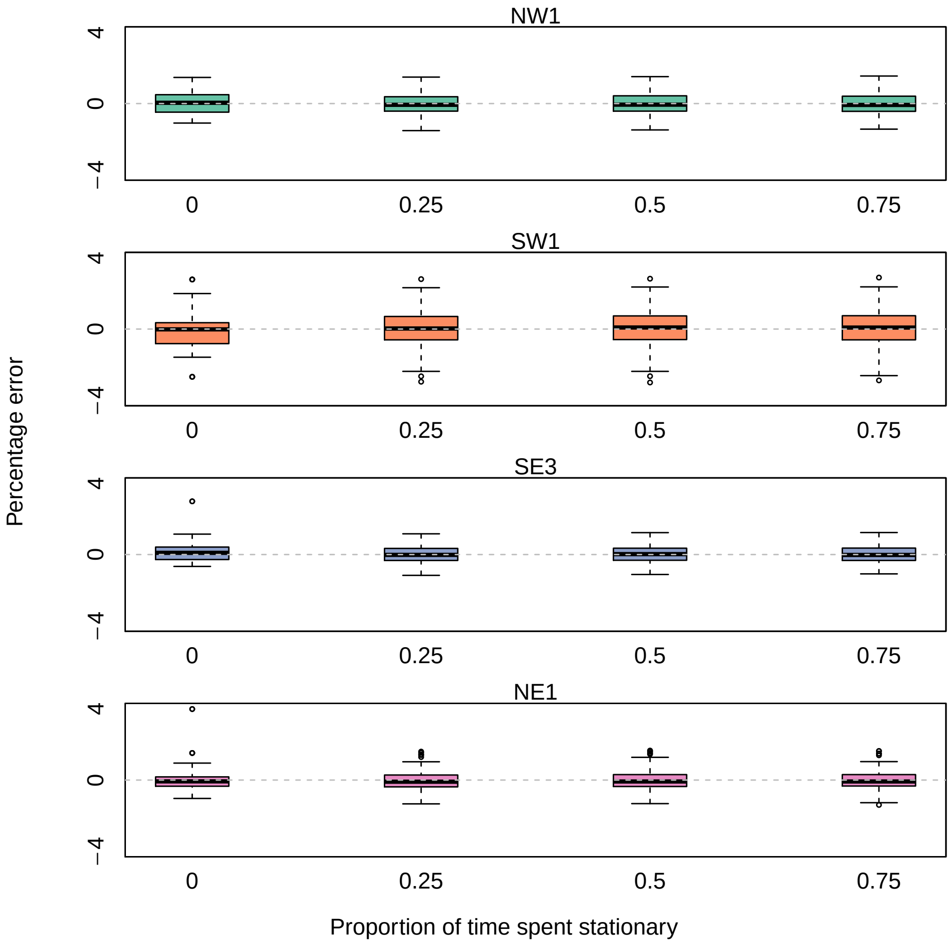

FIGURE 10. Proportion of time spent stationary

FIGURE 11. Accuracy and the precision of the gREM given changes in the amount of time an animal spends stationary on average. Distribution of model error when simulated animals spend increasing proportion of time stationary where: $r = 100\,\text{m}$; $T = 150\,\text{days}$; $v = 40\,\text{km days}^{-1}$; $D = 70\,\text{animals km}^{-2}$; and with detection angles varying between models. Where the model names refer to Figure 1 in Appendix S2.

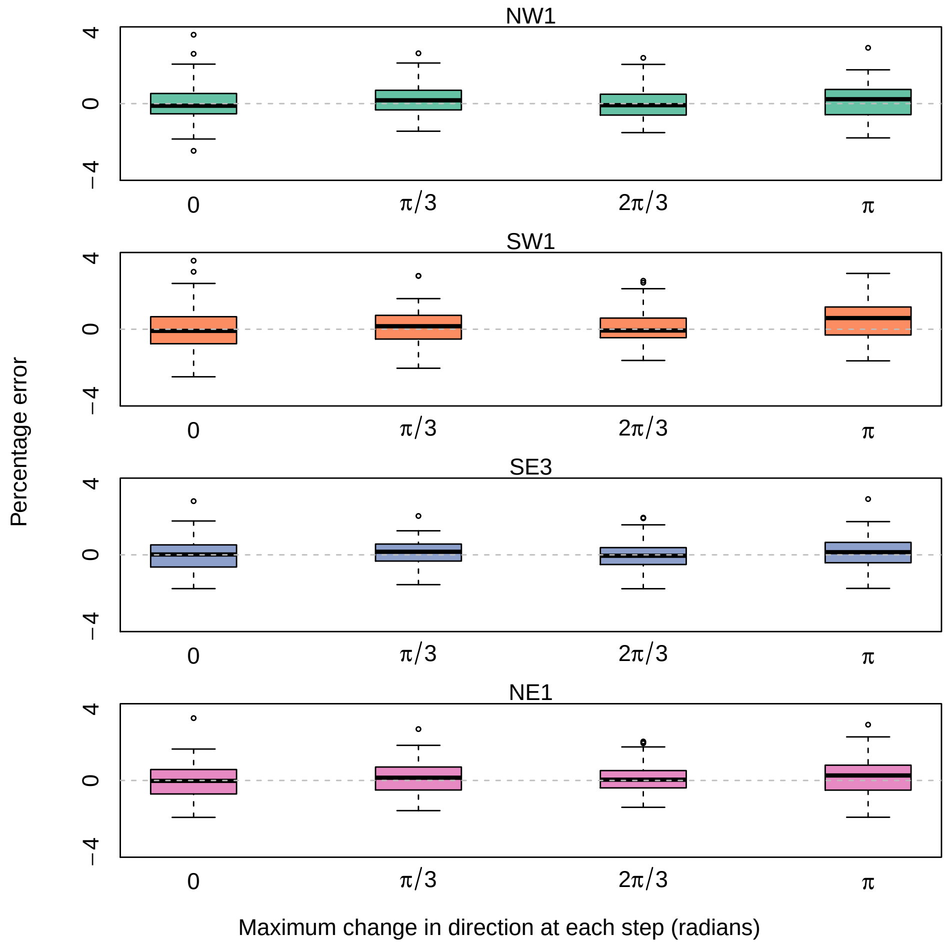

FIGURE 12. Angle of correlated walk

FIGURE 13. Accuracy and the precision of the gREM given different types of correlated walks. Distribution of model error when simulated animals move with different types of correlated walk where: $r = 10\,\mathrm{m}$; $T = 352\,\mathrm{days}$; $v = 40\,\mathrm{km\,days}^{-1}$; $D = 70\,\mathrm{animals\,km}^{-2}$; and with angles varying between models. Where the model names refer to Figure 1 in Appendix S2.